Hydrogen storage in Ti-Fe-Hf alloys: a DFT approach

Robbe Daelman[1], Leander Deleux[2], Zeno Wuyts[2], Abdelali EL OMRANI[3]
[1]*Ghent University*
[2]*Antwerp University and*
[3]*Mohammed VI Polytechnic University, Morocco*
(Dated: December 6, 2025)

In this work, several compounds based on Ti, Fe, Hf, and Ni, along with their solid solutions—including TiFe/$TiFe_2$, HfFe/$HfFe_2$ and TiFeHfNi—were examined for their hydrogen storage capabilities at different Wyckoff positions. The compounds were assessed using formation energies (phase stability diagrams) and the energy cost associated with varying hydrogen concentrations. TiFe, $TiFe_2$, $HfFe_2$ and TiFeHfNi in both cubic and hexagonal symmetries exhibit negative formation energies after hydrogen insertion, indicating thermodynamic stability. In contrast, hydrogen insertion into elemental Ti, Fe, Ni, and Hf generally leads to positive formation energies, except for the Hf structure with hydrogen at the 2a Wyckoff position. Regarding the hydrogen insertion energy, only HfFe and Hf show spontaneous (exothermic) hydrogen absorption behaviour.

I. INTRODUCTION

Hydrogen has the highest specific chemical energy of any element on the periodic table and it is the most abundant element in the universe [1]. Naturally, active research is being performed to use hydrogen to decarbonize the global energy production and storage, as described in [2]. One of the major challenges that must be overcome is the safe and reliable storage of hydrogen. Chemical storage of hydrogen in solid state of metal hydrides is the safest method since these can be functioned at lower pressure and ambient temperature [3].This requires a wide range of operation temperatures, rapid hydrogen sorption kinetics and a significant weight percentage of hydrogen, which has proved to be challenging[1]. A promising class of materials are TiFe based alloys which satisfy the thermodynamic and kinetics requirements, but the capacity still needs to be improved [1]. A major advantage of these materials is that they are cheap to manufacture and can be produced from low cost recycled steel and alloys [4]. However, they must be activated at high temperatures (400-450°C) and high hydrogen pressures (65 kbar), complicating the hydrogenation process. These activation properties can be significantly enhanced by compositional design [1]. For example, simultaneous substitution of Hf and Ni into the TiFe matrix leads to the stabilization of the cubic Pm-3m structure. Specifically $Ti_{0.9}Hf_{0.1}Fe_{0.9}Ni_{0.1}$ shows a strong reduction in activation temperature with only a small reduction in total hydrogen absorption [5]. This paper aims to find the most suitable site and compound amongst Ti-Fe-Hf alloys for hydrogen storage.

II. METHODS

A. Convergence tests

For the convergence tests of the k-point meshes, energy cutoff, and charge-density cutoff, the following procedure was applied. As an example, the procedure for the TiFe crystal is demonstrated; the same methodology was used for all other crystals. Based on the selected pseudopotentials, initial cutoff values of ecutwfc = 64 Ry and ecutrho = 782 Ry were used for the k-mesh convergence test. Several calculations were performed using different k-meshes, and the corresponding total energies and hydrostatic pressures were recorded. The optimized k-points were selected based on the criterion of minimal changes in the total energy (on the order of a few 0.1 mRy) and a variation of maximum 1 kbar in the hydrostatic pressure. Afterwards, ecutwfc was varied using the optimized k-mesh until the same convergence criteria were satisfied. The same process was repeated for ecutrho.

B. Murnaghan equation and energy vs volume fitting

The Murnaghan equation describes the total energy variation as a function of the cell volume and is expressed as follows:

$$E(V) = E_0 + \frac{B_0 V}{B_1}\left(\frac{\left(\frac{V_0}{V}\right)^{B_1}}{B_1 - 1} + 1\right) - \frac{B_0 V_0}{B_1 - 1} \qquad (1)$$

In which E_0, V_0 and B_0 are the total energy, volume, bulk modulus at equilibrium. $B_1 = \frac{\partial B_0}{\partial P}$ is the pressure derivation of bulk modulus at equilibrium.

Using the optimized cutoff energy, charge density, and k-point sampling, the TiFe lattice parameter was varied from 0.85 % a to 1.10 % a in increments of 0.10 % a. The corresponding total energies, illustrated in figure 5, were then used to determine the equilibrium lattice constant by fitting the Murnaghan equation of state. Furthermore, the volume change as a function of cell volume can estimated near equilibrium using the equation:

$$V(P) = V_0\left(1 + P \times \frac{B_1}{B_0}\right)^{-\frac{1}{B_1}} \qquad (2)$$

C. Geometry optimizations and formation energy

Thermodynamic stability of various compounds will be determined by computing their formation energies. The energy of each crystal is minimized by varying the atomic coordinates as well as the cell shape and volume. From this, compounds that could exist in nature could be predicted. From the total energy obtained from the DFT calculation, the formation energy per atom of the crystals was calculated using equation.

$$E_f = \frac{E_{tot} - \sum_i x_i E_i}{\sum_i x_i} \tag{3}$$

With E_i presents the energy per atom of the pure i element and x_i indicates the number of corresponding atoms in the formula unit.

D. Adding a hydrogen atom

The insertion of hydrogen atom into the TiFe compound can be done by placing H atom in different Wyckoff positions so that the symmetry of the crystal is maintained. In this way the resulting structure will still belong to the same space group. First, the converged settings was checked followed by full geometry optimisation. From this, the formation energy per atom and the weight percentage of H in the crystal can be obtained. In addition, the energy cost per adding one hydrogen atom was also calculated as follows:

$$E_{N\cdot H} = \frac{E_{S@H} - E_S - \frac{N}{2}E(H_2)}{N} \tag{4}$$

Where, $E_{S@H}$, E_S and $E(H_2)$ are the total energies of system with N hydrogen atoms inserted, parent system and hydrogen molecule, respectively.

E. Phase diagrams

A rigorous framework that reveals whether a compound is stable relative to all possible competing phases is a phase diagram. Only hydrides that lie on or near the convex hull within 5 meV can can be considered stable [6]. This is why several phase diagrams were made for analysing the results and determining which crystals are still stable after hydrogen insertion.

All phase diagrams were made according to [7] and [8]. Their existing phase diagrams work based on formation energies that were adapted to fit the experimental formation energies.

F. Adding hydrogen to different crystals

The same procedure discussed in II C and II D was adapted for other compounds in different crystal structures, and for a different hydrogen concentration. In principle, this can be done for every combination of compound, crystal structure, Wyckoff site and amount of hydrogen atoms. However, since this amounts to a very large number of possible configurations, only a small subset of these combinations was studied. The subset uses all previously computed crystals, a few different hydrogen atoms (1,2,3,6, and 8) but only a few Wyckoff sites. The reason for this is that adding too many hydrogen atoms to a crystal structure will render it unstable (as one can intuitively imagine), hence one only needs a maximum of a few (here 8) possible sites for a given crystal. This can be done by only using lower multiplicity Wyckoff sites.

For each configuration, the formation energy per atom was computed using equation 3, along with the hydrogen weight percentage, which remains low due to the high atomic mass of the metals and the limited number of available H-sites. In addition, the incremental energy cost of inserting one hydrogen atom was evaluated using equation 4.

To check the predictions of [5] about $Ti_{0.9}Hf_{0.1}Fe_{0.9}Ni_{0.1}$, a 1x2x5 supercell was constructed. In this way, there are exactly 10 Ti and 10 Fe atoms present, one of which can then be substituted for Hf and Ni respectively.

III. RESULTS

A. Murnaghan equation and energy vs volume fitting

From fitting Murnaghan equation 1, the equilibrium lattice parameter and volume were found to be 2.959 Å and 25.916 Å^3 (12.96 Å^3 for primitive volume), respectively. This lattice parameter is in excellent agreement with the value obtained from the vc-relax calculation (2.954 Å), with a very small difference of only 0.005 Å. Moreover, from the fitted Murnaghan equation of state, the bulk modulus and its pressure derivative at equilibrium were estimated to be 380.7 GPa (190.35 GPa for primitive cell) and 3.54, respectively. The equilibrium lattice parameter and bulk modulus are in close agreement with the Materials Project database values of 2.94 Å and 199 GPa, respectively [9]. Furthermore, based on equation 2, it was estimated that the volume at 10 GPa decreases to 24.699 Å^3, corresponding to a 4.7% reduction relative to the equilibrium volume of the primitive cell.

B. Full geometry optimizations

In table I the energies of the four pure crystals are found as well as the formation energies of the compounds.

It can be seen that all formation energies are negative, which means the compounds are exothermic to form from

TABLE I. Energy per atom and formation energies of pure elements and compounds

Crystal	Space group	Energy/atom (eV)	E_f (eV)
Ti	P6/mmm	-1622.493816	–
Fe	Im3m	-4479.97283	–
Hf	$P6_3/mmc$	-1535.137521	–
Ni	Fm3m	-4669.543389	–
TiFe	Pm-3m	-3051.66408	-0.431
$HfFe_2$	$P6_3/mmc$	-3498.70200	-0.341
$HfFe_2$	Fd-3m	-3498.71743	-0.356
$TiFe_2$	$P6_3/mmc$	-3527.77484	-0.295
$TiFe_2$	Fd-3m	-3527.78580	-0.306
HfFe	Pm-3m	-3007.88670	-0.332

their constituent elements. However, this does not necessarily mean that the compounds are found in nature, since configurations with even lower energy may exist, in which case those configurations would be observed instead. From [10], it is observed that the formation energy of TiFe lies close to the literature value of $-0.421, \mathrm{eV}$, which lies on the hull and therefore indicates that the compound is stable. Note that this is not a experimental value but also calculated with a DFT code. The results obtained from the DFT code are simulated at 0 Kelvin, while the experimental phase diagrams are usually around room temperature and higher. It is therefore not useful to compare exact values, but it can be useful for relative differences and the sign of the formation energy. The experimental Ti–Fe phase diagram [11] shows that TiFe is the broadest and thermodynamically most stable intermetallic phase. $TiFe_2$ also exist, but has a smaller stability range and occur mainly at lower temperatures. This matches the trend of the results for our DFT code. According to [12], $HfFe_2$ is also a stable state, which is consistent with our result. However, HfFe is not listed here as a stable state.

C. Adding one hydrogen atom

Using equation 3 and 4, the formation energy and the energy cost of adding hydrogen was calculated. For TiFe with one hydrogen atom was added at the 3c and 3d Wyckoff positions and the corresponding formation energies were found to be -0.2911649903 eV and -0.282930699 eV, respectively, consistent with literature finding of -0.233 eV [13]. For the energy cost per hydrogen, a value of -0.01198546872 eV for 3c and 0.01271740525 eV for 3d was obtained. Resulting in that 3c is the most stable.

D. Phase Diagrams

Several phase diagrams were made in 2D, 3D and 4D. The TiFeH and TiFeHfH phase diagrams will be discussed here. All other phase diagrams can be found in the appendix. When adding hydrogen, a 3D phase diagram is obtained. The Gibbs' triangle can be seen in figure 1. All green dots correspond to the crystals that would still be stable with hydrogen inside, relative to the other phases. Of all crystals that are shown here, $TiFe_2H$ seems like the most stable one to store hydrogen. FeH and TiH lie on the lines between the pure element and hydrogen. They have positive formation energies and aren't suitable candidates to store hydrogen. TiFeH is the red dot below $TiFe_2H$. It has a negative formation energy, but it is less favourable than $TiFe_2H$ and will therefore decompose. A 4D Gibbs' tetrahedron is shown for TiFeHfH in figure 2. Again, multiple crystals with hydrogen inside seem to be stable. Of all binary crystals with hydrogen, only HfH is stable. It's formation energy is only slightly negative though. $TiFe_2H$, TiFeH and HfFeH are the most stable crystals with hydrogen. Multiple other crystals with hydrogen also have negative formation energies, but will nevertheless decompose into other more stable crystals.

For the crystals without hydrogen, the average difference between the formation energies in this paper and in the reference phase diagrams [7], [8] is 0.008 eV/atom. Comparing the crystals with hydrogen is more difficult, because the reference data does not provide space groups, Wyckoff positions, etc.

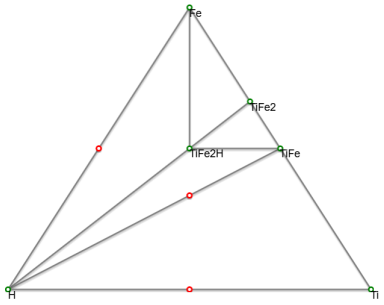

FIG. 1. 3D phase diagram of TiFeH. All simulated crystals containing Ti, Fe and/or H are portrayed on the Gibbs' triangle. The three pure crystals are located in the corners. The position between the crystals represents the ratio between the different elements. All green points are stable, the red points are the simulated crystals that are unstable.

E. Adding hydrogen to different crystals

The formation energies and hydrogen weight percentages are shown in figure 3. One can see a general trend of the crystals being less stable when a higher weight percentage of hydrogen is added, which is what one intuitively expects. One notable exception to this rule is the TiFe crystal, which only contains 2 atoms (1 Ti, 1 Fe) in the unit cell and is hence able to attain a higher hydrogen weight percentage. On the other hand, the Ni crystals seem to be particularly unstable when hydrogen is added. All $HfFe_2$ and $TiFe_2$ crystals had a negative formation energy for the given hydrogen count and Wyckoff

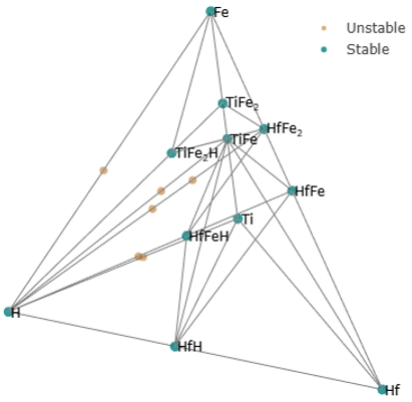

FIG. 2. 4D phase diagram of TiFeHfH. All crystals containing Ti, Fe, Hf and/or H are portrayed on the Gibbs' tetrahedron. The four pure crystals are located in the corners. The position between the crystals represents the ratio between the different elements. All green points are stable, the brown points are the simulated crystals that are unstable.

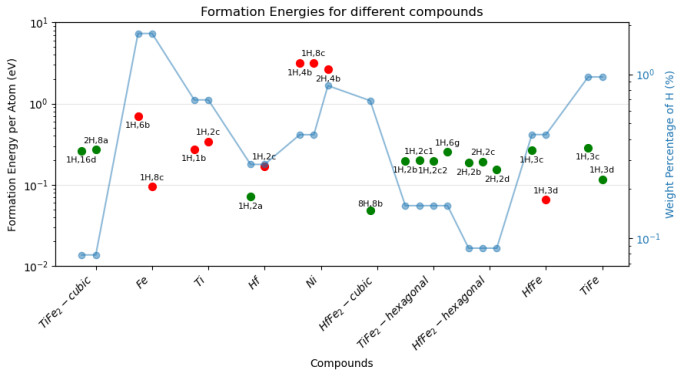

FIG. 3. Formation energies and hydrogen weight percentages for different compounds. The x axis shows the name (and configuration if multiple were used) of the compounds, the Wyckoff sites and amount of Hydrogen atoms are indicated next to the data points. The energy axis is shown on the left, green data points indicate negative formation energies and hence stable compounds, red points indicate positive and hence unstable compounds. The y axis on the right shows the weight percentage of hydrogen in the compound. There is a blue data point corresponding to every red/green data point.

sites.

The energy cost per hydrogen atom added to the crystal is shown in figure 4. Only for the Hf crystal with Wyckoff site 2a and the HfFe crystal with Wyckoff site 3c does it seem to be energetically favourable to absorb hydrogen, and even in these cases the energy cost per hydrogen atom is only slightly negative. Some of the other crystals, like TiFe with Wyckoff site 3c only need a small amount of energy to absorb a hydrogen atom. From this, one can conclude that the 3c Wyckoff site in the Pm-3m seems to be a particularly stable site to put hydrogen in and that Hf seems to be the most favourable element to host hydrogen. On the other hand, the extremely stable Fe crystal is a highly unfavourable environment for hydrogen atoms. Finally, it should be noted that in crystals with multiple hydrogen atoms, the average cost per hydrogen atom added will inevitably be higher, since it takes more energy every time an atom is added. Using supercells, $Ti_{0.9}Hf_{0.1}Fe_{0.9}Ni_{0.1}$ alloys with respectively 10, 15 and 20 hydrogen atoms were studied as well. All of those crystals had negative formation energies. However, the cost of adding hydrogen was positive. Therefore, these alloys don't seem to be the best choice for hydrogen storage and are hence not in the figures.

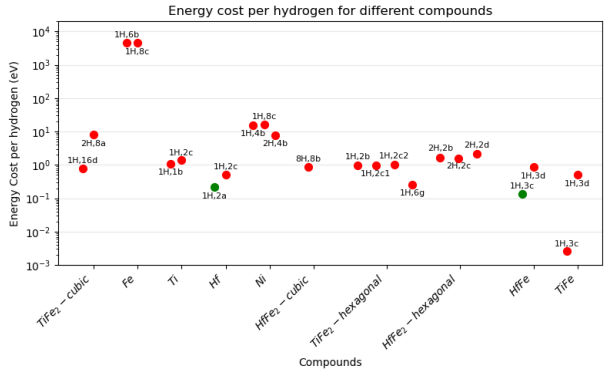

FIG. 4. The energy cost per hydrogen atom for different compound. The x axis once again labels the different compounds and configurations, the y axis shows the average energy cost for adding a hydrogen atom to that compound. The Wyckoff sites and amount of hydrogen atoms are shown next to the data points. A red data point indicates a positive energy cost per hydrogen, a green data point indicates a negative energy cost per hydrogen.

IV. CONCLUSION

After performing a full geometry optimisation of all crystals, hydrogen could be added. Next the formation energy and energy cost per hydrogen atom could be determined. A phase diagram analysis concluded that $TiFe_2H$, TiFeH, HfFeH and TiFeHfNi were the most energetically stable crystals to store hydrogen from all TiFeHfH compounds. Both FeH and TiH have a positive formation energy and are not suitable to store hydrogen.

When looking at the energy cost per added hydrogen atom, it turns out that the 2a Wyckoff site of Hf and the 3c Wyckoff site of HfFe gain energy when storing 1 hydrogen atom in the crystal. Adding 1 hydrogen atom to the 3c Wyckoff site of TiFe only requires a small amount of energy, so these crystals seem the most suited for hydrogen storage. Finally, it turns out that storing a higher weight percentage of hydrogen makes the crystals more unstable, with the exception of TiFe which was able to obtain about 1 wt% hydrogen with a similar (negative) formation energy as the other crystals.

[1] H. Liu, J. Zhang, P. Sun, C. Zhou, Y. Liu, and Z. Z. Fang, An overview of tife alloys for hydrogen storage: Structure, processes, properties, and applications, Journal of Energy Storage **68**, 107772 (2023).

[2] I. Staffell, D. Scamman, A. Velazquez Abad, P. Balcombe, P. E. Dodds, P. Ekins, N. Shah, and K. R. Ward, The role of hydrogen and fuel cells in the global energy system, Energy Environ. Sci. **12**, 463 (2019).

[3] G. K. Sujan, Z. Pan, H. Li, D. Liang, and N. Alam, An overview on tife intermetallic for solid-state hydrogen storage: microstructure, hydrogenation and fabrication processes, Critical Reviews in Solid State and Materials Sciences **45**, 410 (2020), https://doi.org/10.1080/10408436.2019.1652143.

[4] Y. Shang, S. Liu, Z. Liang, *et al.*, Developing sustainable FeTi alloys for hydrogen storage by recycling, Communications Materials **3**, 101 (2022).

[5] K. Komedera, J. Michalik, K. Sworst, and Gondek, Structure, microstructure and hyperfine interactions in hf- and ni-substituted tife alloy for hydrogen storage, Acta Physica Polonica A **146**, 215 (2024).

[6] P. Y. Chew and A. Reinhardt, Phase diagrams—why they matter and how to predict them, The Journal of Chemical Physics **158**, 030902 (2023).

[7] S. Kirklin, J. E. Saal, B. Meredig, A. Thompson, J. W. Doak, M. Aykol, S. Rühl, and C. Wolverton, The open quantum materials database (oqmd): assessing the accuracy of dft formation energies, npj Computational Materials **1** (2015).

[8] J. E. Saal, S. Kirklin, B. Meredig, M. Aykol, and C. Wolverton, Materials design and discovery with high-throughput density functional theory: The open quantum materials database (oqmd), JOM **65** (2013).

[9] A. Jain, S. P. Ong, G. Hautier, W. Chen, W. D. Richards, S. Dacek, S. Cholia, D. Gunter, D. Skinner, G. Ceder, and K. A. Persson, Commentary: The materials project: A materials genome approach to accelerating materials innovation, APL Materials **1**, 011002 (2013), https://pubs.aip.org/aip/apm/article-pdf/doi/10.1063/1.4812323/13163869/011002$_1$*online.pdf*.

[10] MaterialsProject, Ti–fe phase diagram (2024), accessed: 2024-02-20.

[11] J. L. Murray *et al.*, Fe–ti phase diagram, Online figure, reproduced from ref. 25/26 (1990), accessed via ResearchGate figure link.

[12] O. K. von Goldbeck, Fe—hf iron—hafnium, in *IRON—Binary Phase Diagrams* (Springer Berlin Heidelberg, Berlin, Heidelberg, 1982) pp. 50–51.

[13] L. Mohammedi, B. Daoudi, A. Boukraa, and H. Chaib, Structural and electronic properties of the ternary intermetallic hydride tifeh from ab-initio calculations, Annales des Sciences et Technologie **7**, 108 (2016).

[14] P. Giannozzi, S. Baroni, N. Bonini, M. Calandra, R. Car, C. Cavazzoni, D. Ceresoli, G. L. Chiarotti, M. Cococcioni, I. Dabo, A. Dal Corso, S. de Gironcoli, S. Fabris, G. Fratesi, R. Gebauer, U. Gerstmann, C. Gougoussis, A. Kokalj, M. Lazzeri, L. Martin-Samos, N. Marzari, F. Mauri, R. Mazzarello, S. Paolini, A. Pasquarello, L. Paulatto, C. Sbraccia, S. Scandolo, G. Sclauzero, A. P. Seitsonen, A. Smogunov, P. Umari, and R. M. Wentzcovitch, Quantum espresso: a modular and open-source software project for quantum simulations of materials, Journal of Physics: Condensed Matter **21**, 395502 (2009).

[15] M. Ernzerhof and G. E. Scuseria, Assessment of the perdew–burke–ernzerhof exchange-correlation functional, The Journal of Chemical Physics **110**, 5029 (1999), https://pubs.aip.org/aip/jcp/article-pdf/110/11/5029/19111374/5029$_1$*online.pdf*.

[16] G. Prandini, A. Marrazzo, I. E. Castelli, N. Mounet, and N. Marzari, Precision and efficiency in solid-state pseudopotential calculations, npj Computational Materials **4**, 72 (2018).

APPENDIX

In this study, Density Functional Theory (DFT) as implemented in the Quantum ESPRESSO package was used for all calculations [14]. The exchange–correlation interaction was treated using the PBE functional [15]. The electron–ion interaction was described using pseudopotentials from the SSSP library [16].

TABLE II. Convergence testing of K-mesh for TiFe crystal

K-mesh	Energy (Ry)	Pressure (kbar)
5x5x5	-448.58105175	16.42
6x6x6	-448.57714803	26.77
7x7x7	-448.57874081	19.74
8x8x8	-448.57892115	21.32
9x9x9	-448.57928947	21.38
10x10x10	-448.57953964	19.65
11x11x11	-448.57917501	21.20
12x12x12	-448.57935381	20.95
13x13x13	-448.57929875	20.75
14x14x14	-448.57935518	20.67
15x15x15	-448.57935461	20.86

TABLE III. Convergence testing of ecutwfc for TiFe crystal

ecutwfc	Energy (Ry)	Pressure (kbar)
54	-448.57697351	23.45
64	-448.57935381	20.95
74	-448.58322087	18.64
84	-448.58548329	27.31
94	-448.58598736	32.32
104	-448.58608342	31.37
114	-448.58631836	30.41
124	-448.58659310	30.78
134	-448.58674456	31.52

TABLE IV. Convergence testing of ecutrho for TiFe crystal

ecutrho	Energy (Ry)	Pressure (kbar)
624	-448.58607284	31.09
728	-448.58610547	31.45
832	-448.58607018	31.44
936	-448.58607147	31.21
1040	-448.58607168	31.51
1144	-448.58606437	31.76
1248	-448.58606543	31.18

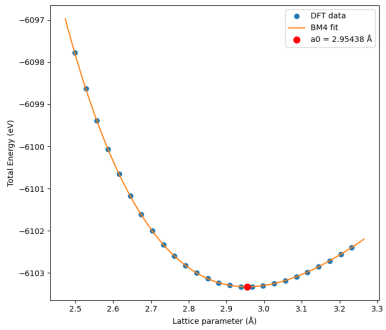

FIG. 5. DFT total energy of the material as a function of lattice parameter (blue dots). The solid orange line represents a 4th-order Birch–Murnaghan equation of state fit to the DFT data. The equilibrium lattice parameter, corresponding to the minimum total energy, is highlighted with a red dot.

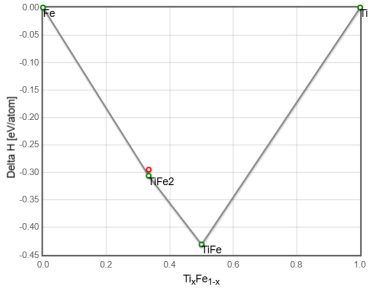

FIG. 6. 2D phase diagram of TiFe. All simulated crystals containing Ti and/or Fe are portrayed. On the horizontal axis the amount of Ti is shown. Delta H is the formation energy in eV/atom on the vertical axis. All green points lie on the convex hull and are stable. The red points are simulated crystals that are unstable.

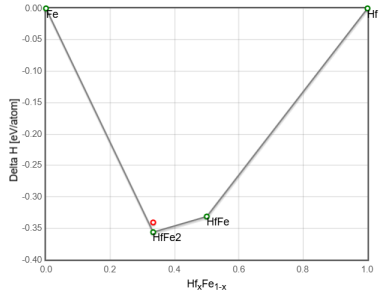

FIG. 7. 2D phase diagram of HfFe. All simulated crystals containing Hf and/or Fe are portrayed. On the horizontal axis the amount of Ti is shown. Delta H is the formation energy in eV/atom on the vertical axis. All green points lie on the convex hull and are stable. The red points are simulated crystals that are unstable.

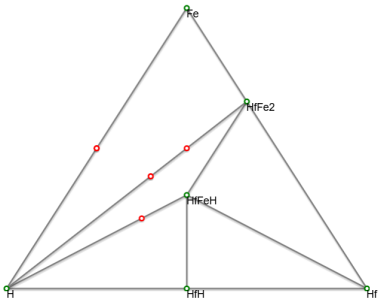

FIG. 8. 3D phase diagram of HfFeH. All simulated crystals containing Hf, Fe and/or H are portrayed on the Gibbs' triangle. The three pure crystals are located in the corners. The position between the crystals represents the ratio between the different elements. All green points are stable, the red points are the simulated crystals that are unstable.

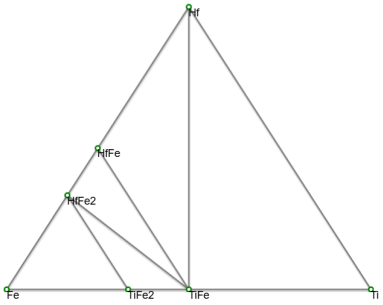

FIG. 9. 3D phase diagram of TiFeHf. All simulated crystals containing Ti, Fe and/or Hf are portrayed on the Gibbs' triangle. The three pure crystals are located in the corners. The position between the crystals represents the ratio between the different elements. All green points are stable, the red points are the simulated crystals that are unstable.

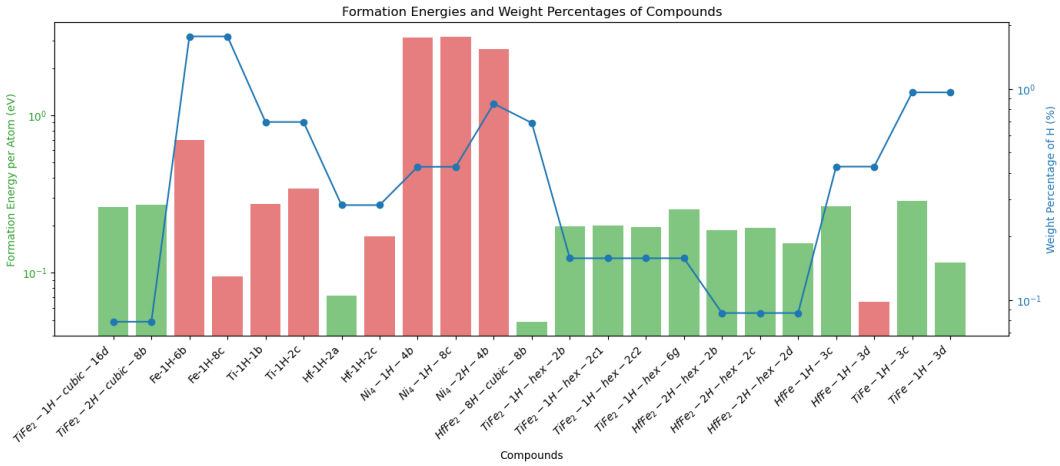

FIG. 10. Calculated formation energies and hydrogen weight percentage for different configurations. The left y axis shows the formation energy in log scale, negative formation energies (stable) are shown in green and positive formation energies (unstable) are shown in red. The right y axis shows the weight percentage of hydrogen in the compound, again on a log axis.

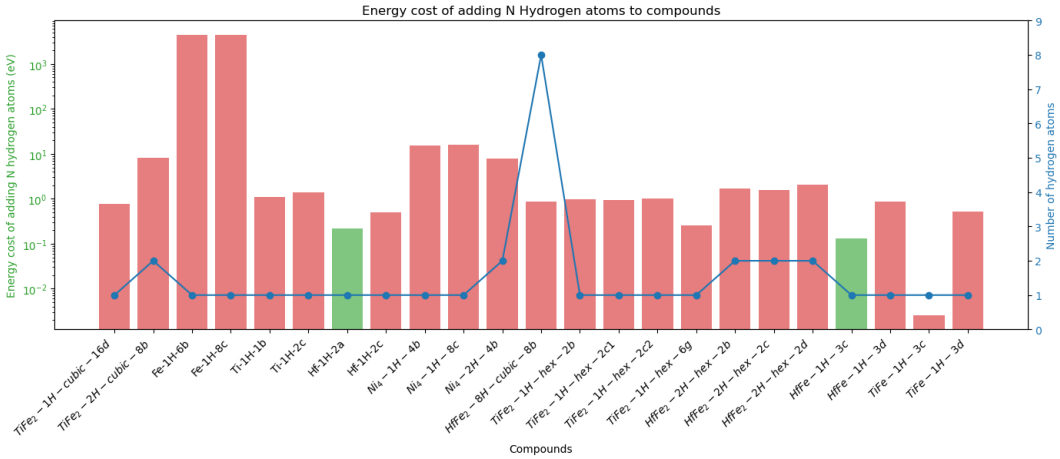

FIG. 11. Calculated energy cost per added hydrogen atom and number of added hydrogen atoms for different configuration. The left y axis shows the energy cost in log scale, negative energy costs (more stable) are shown in green and positive energy costs (less stable) are shown in red. The right y axis shows the amount of hydrogen atoms in the unit cell.